Tectonic Evolution of the Condrey Mountain Schist: an Intact Record of Late Jurassic to Early Cretaceous Franciscan Subduction and Underplating

C. M. Tewksbury-Christle[1], W. M. Behr[2], M. A. Helper[3], and D. F. Stockli[3]

[1]Geosciences Department, Fort Lewis College, 1000 Rim Drive, Durango, CO, 81301
[2]Structural Geology and Tectonics Group, Geological Institute, Department of Earth Sciences, ETH Zurich, Sonneggstrasse 5, 8092 Zurich, Switzerland
[3]Department of Earth and Planetary Sciences, Jackson School of Geosciences, University of Texas at Austin, 2305 Speedway Stop C1160, Austin, TX 78712

Key Points:

- The Condrey Mountain Schist (CMS) epidote-blueschist facies rocks were deposited and underplated in the Late Jurassic to Early Cretaceous.
- Underplating postdates Klamath terrane assembly and predates coherent Franciscan underplating, recording the early Franciscan history.
- CMS pressure-temperature conditions are consistent with other estimates of early Franciscan subduction zone thermal structure.

Corresponding author: Carolyn Tewksbury-Christle, `cmtewksburychristl@fortlewis.edu`

Abstract

The Klamath Mountains in northern California and southern Oregon are thought to record 200+ m.y. of subduction and terrane accretion, whereas the outboard Franciscan Complex records classic ocean-continent subduction along the North American margin. Unraveling the Klamaths' late history could help constrain this transition in subduction style. Key is the Mesozoic Condrey Mountain Schist (CMS), comprising, in part, a subduction complex that occupies a structural window through older, overlying central Klamath thrust sheets but with otherwise uncertain relationships to other, more outboard Klamath or Franciscan terranes. The CMS consists of two units (upper and lower), which could be correlated with 1) other Klamath terranes, 2) the Franciscan, or 3) neither based on regional structures and limited extant age data. Upper CMS protolith and metamorphic dates overlap with other Klamath terranes, but the lower CMS remains enigmatic. We used multiple geochronometers to constrain the timing of lower CMS deposition and metamorphism. Maximum depositional ages (MDAs) derived from detrital zircon geochronology of metasedimentary rocks are 153-135 Ma. Metamorphic ages from white mica K-Ar and Rb-Sr multi-mineral isochrons from intercalated and coherently deformed metamafic lenses are 133-116 Ma. Lower CMS MDAs (<153 Ma) predominantly postdate the age of other Klamath terranes, but subduction metamorphism appears to predate the earliest coherent Franciscan underplating (ca. 123 Ma). The lower CMS thus occupies a spatial and temporal position between the Klamaths and Franciscan and preserves a non-retrogressed record of the Franciscan Complex's early history (>123 Ma), otherwise only partially preserved in retrogressed Franciscan high grade blocks.

1 Introduction

The Klamath Mountains of northern California and southern Oregon expose rocks that record protracted subduction from the Early Devonian to the Late Jurassic (Snoke & Barnes, 2006). The rocks of the Klamaths are bounded on the west by the younger Franciscan Complex, which records subduction from the Middle Jurassic to the Eocene (Fig. 1a-b) (e.g., Bailey et al., 1964; Evitt & Pierce, 1975; Dumitru et al., 2010; Morissani, 2006; Hopson et al., 2008; Shervais & Choi, 2012), and on the east and south by a Cretaceous to Tertiary onlap sequence (Nilsen, 1984; Snoke & Barnes, 2006). The Klamaths consist primarily of broadly eastward-dipping, westward-younging thrust sheets that represent suprasubduction zone terranes telescoped onto the North American margin (e.g., Saleeby, 1990; Hacker et al., 1995; Snoke & Barnes, 2006). Because terrane accretion plays a key role in long-term growth of continental crust, significant effort has gone into unraveling the complex tectonic history of the Klamaths, including, for example, the origin of ophiolitic terranes (Wright & Wyld, 1994; Gray, 1986; Yule et al., 2006; Harper et al., 1994), the ages and styles of arc magmatism (Allen & Barnes, 2006; Barnes et al., 2006; Bushey et al., 2006; Harper, 2006; McFadden et al., 2006), and the timing and mechanisms of terrane accretion and continental growth (Helper, 1986; Saleeby & Harper, 1993; Hacker et al., 1995; Gray, 2006; Pessagno, 2006; Snoke & Barnes, 2006) (Fig. 1b). The timing of deposition, subduction, and metamorphism of the structurally lowest unit in the central Klamaths, the Condrey Mountain Schist (Figs. 1b and 2), however, remains enigmatic.

How the Condrey Mountain Schist (CMS) fits into the complex regional tectonics of the Klamaths and the outboard Franciscan Complex is currently unresolved. The CMS principally occupies a large structural window through older greenschist to amphibolite facies Klamath terranes (Fig. 1c) (Helper, 1985, 1986; Saleeby & Harper, 1993; Snoke & Barnes, 2006), but subordinately also occurs within a small thrust sheet beneath these same rocks in the Klamath River canyon about 15 km west of the window (Hill, 1985). It consists of a greenschist- to epidote-amphibolite-facies unit (upper CMS), structurally underlain by epidote-blueschist facies rocks (lower CMS) that record the progressive underplating at 30-40 km depth of dominantly oceanic-affinity sedimentary protoliths, with m- to km-scale lenses of mafic and ultramafic protoliths (Fig. 2) (Helper, 1986; Tewksbury-Christle et al., 2021). Previous researchers connected the CMS to forearc- and arc-related terranes in the Klamaths (Fig. 1b) based on regional relationships (e.g., Saleeby & Harper, 1993). However, previously published or cited emplacement or metamorphic ages for the lower CMS range from 167 ± 12 Ma to 118 ± 2 Ma (Hacker et al., 1995; Saleeby & Harper, 1993; Helper, 1986; Coleman et al., 1983), overlapping in time with both the youngest Klamath terranes and the oldest Franciscan units, therefore providing poor constraints on regional correlations and relationships. Resolving this issue will allow better constraints on the transition from outboard subduction and terrane accretion to the unimpeded ocean-continent subduction recorded by the Franciscan Complex.

In order to resolve the tectonic evolution of the CMS, we employ multiple geochronometers to constrain the provenance and depositional ages (where applicable) of different protoliths within the lower CMS, along with the timing of metamorphism as a function of structural depth over the full thickness of the exposed lower CMS. We use these new datasets to place constraints on the timing of lower CMS deposition, subduction, and underplating, and we discuss the broader regional implications for the Klamaths and Franciscan Complex in the context of Western North America Cordilleran convergent tectonics.

2 Tectonic Setting

2.1 Klamath Mountains

The Klamath Mountains record Early Devonian through Early Cretaceous subduction and subsequent accretion of multiple fringing island arc systems onto the western margin of North America (Fig. 1b) (e.g., Snoke & Barnes, 2006; Saleeby, 1990; Hacker et al., 1995; Saleeby & Harper, 1993; Helper, 1986; Irwin, 1972). These terranes include arc-related units, forearc and backarc basinal deposits, ophiolites, and fossil accretionary wedges (e.g., Gray, 1986; Saleeby, 1990; Saleeby & Harper, 1993; Wright & Wyld, 1994; Hacker et al., 1995; Gray, 2006; Pessagno, 2006; Snoke & Barnes, 2006; Yule et al., 2006). Timing of formation and/or deposition of the Klamath terranes is well-constrained, as is motion on the suturing thrust faults, but similar age constraints do not exist for the CMS.

The CMS occupies a similar structural position as the Western Klamath terrane, with the majority of the window-bounding faults placing the Rattlesnake Creek terrane on top of the CMS, much like the Orleans fault places the Rattlesnake Creek on top of the Western Klamath terrane (Fig. 1b-c). The Rattlesnake Creek terrane (with components that range in age from 161-300 Ma) is floored by a Late Triassic ophiolitic melange, locally at amphibolite facies, with thin volcanic cover sequences that are overlain by the Western Hayfork arc volcanics (169-179 Ma) (Wright, 1982; Gray, 1986; Hacker et al., 1995; Snoke & Barnes, 2006; Barnes et al., 2006; Frost et al., 2006; LaMaskin et al., 2021). The Rattlesnake Creek/Western Hayfork terranes sutured to the inboard Klamath terranes ca. 170 Ma (Saleeby, 1990; Snoke & Barnes, 2006) and underwent transtensional forearc spreading that resulted in formation of the Josephine Ophiolite (161-165 Ma) (Saleeby & Harper, 1993; Hacker et al., 1995; Snoke & Barnes, 2006; Yule et al., 2006). The Galice Formation flysch (part of the Western Klamath terrane; Figure 1b) was deposited in the Josephine basin following spreading (151-158 Ma) (Frost et al., 2006; Macdonald et al., 2006; LaMaskin et al., 2021; Surpless et al., 2023). Onlap and interfingering of the Galice with the Rogue-Chetco arc volcanics (155-160 Ma) indicate a transition of the active arc from the Western Hayfork to a location farther outboard as a consequence of forearc spreading (Snoke & Barnes, 2006; Yule et al., 2006), transitioning the Josephine-Galice basins from the forearc to the backarc. The Western Klamath terrane was thrust under the Western Hayfork and Rattlesnake Creek terranes along the Orleans fault (ca. 153-150 Ma, well-constrained by rootless and cross-cutting plutons) (Snoke & Barnes, 2006; Frost et al., 2006; Saleeby, 1990). Although plutonic activity continued until ca.

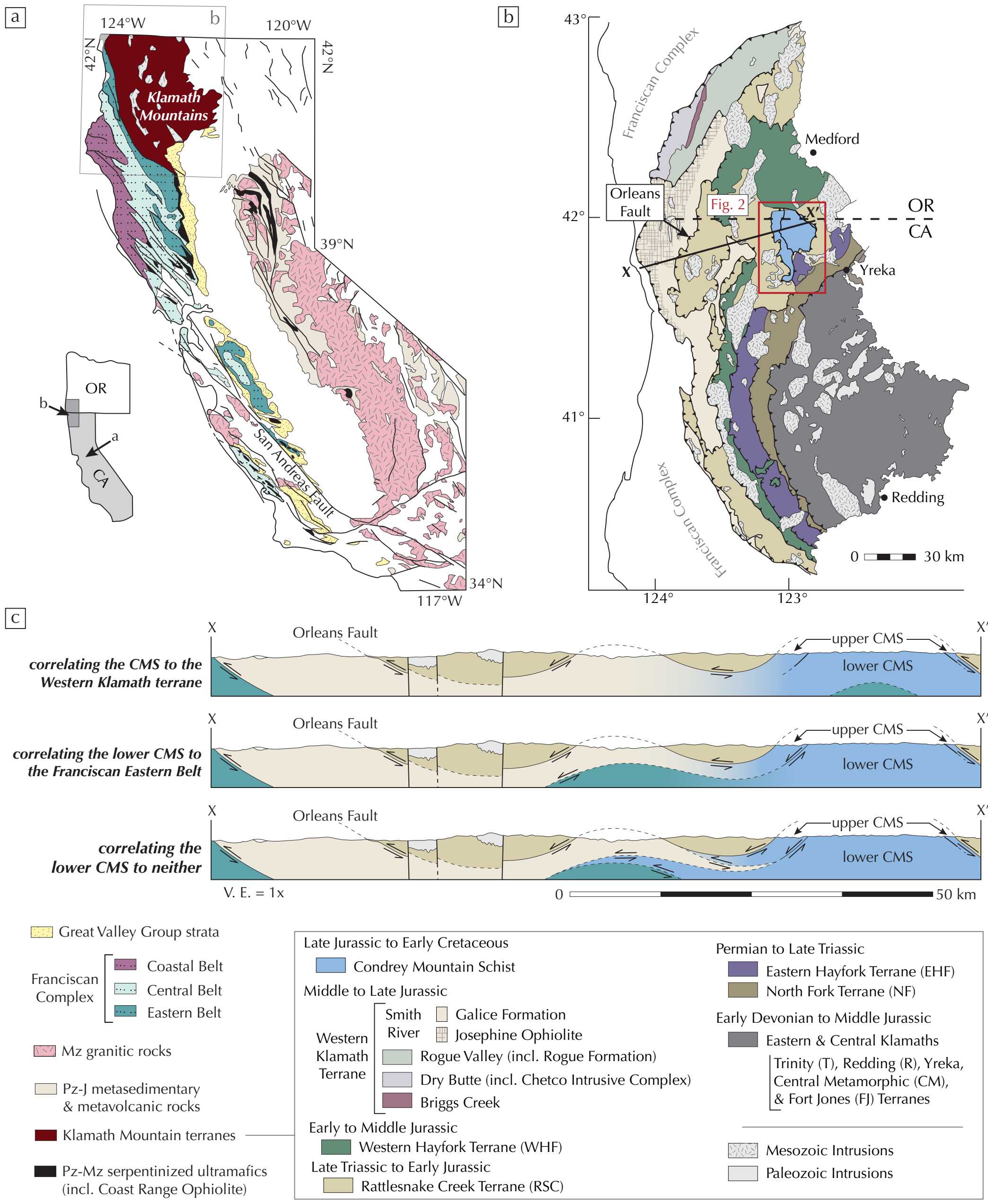

Figure 1. a) Regional geologic map of the Klamaths and the younger, outboard accretionary wedge-forearc-arc system preserved in the Franciscan Complex, Great Valley Group, and Sierra Nevada (after Ernst, 2015). b) Geologic map of the Klamath terranes (after Snoke & Barnes, 2006; Tewksbury-Christle et al., 2021). c) Cross-sections along X-X' (after Saleeby & Harper, 1993) illustrating three possible correlations of the CMS based on regional relationships and limited extant age constraints.

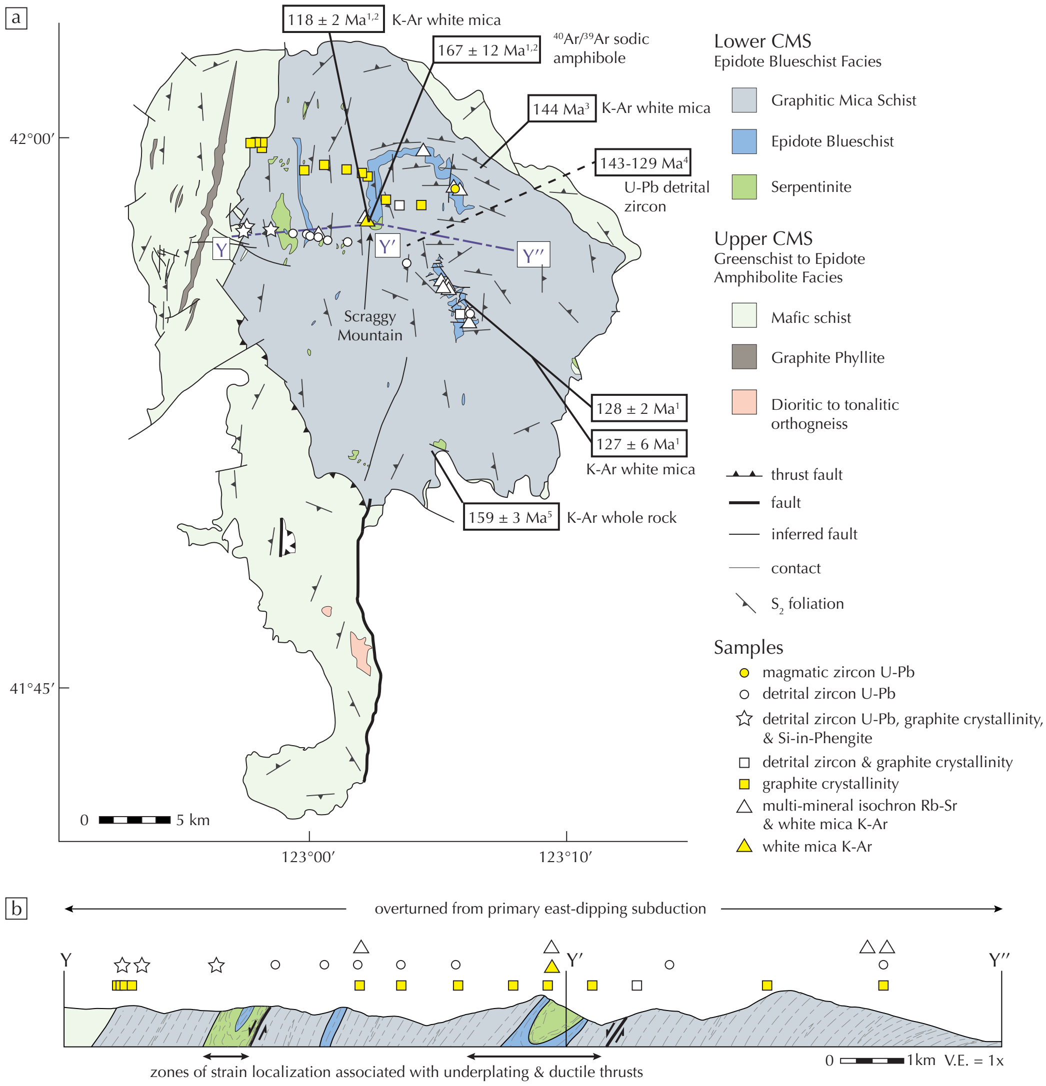

Figure 2. Geologic map (a) and cross section (b) of the CMS showing sample locations for magmatic and detrital zircon U-Pb, white mica K-Ar, multi-mineral isochron Rb-Sr, graphite crystallinity, and Si-in-phenigite (after Tewksbury-Christle et al., 2021). We projected samples onto the cross section where necessary using the pervasive S_2 foliation. Previously published CMS dates are from Helper (1986)[1], Coleman et al. (1983)[2], Lanphere et al. (1968)[3], Chapman et al. (2021)[4] taken across a transect, and Suppe and Armstrong (1972)[5].

136 Ma and migrated progressively eastward (Allen & Barnes, 2006), the Orleans fault has traditionally been interpreted as the final suturing event of the Klamath terranes (e.g., Snoke & Barnes, 2006, and references therein).

Eastward subduction along the western margin of North America continued after emplacement of the above-mentioned Klamath terranes, as recorded in the primarily younger, outboard Franciscan Complex and the associated forearc deposition (Great Valley Group) and arc magmatism (Sierra Nevada batholith) (Fig. 1a) (e.g., Bailey et al., 1964; Evitt & Pierce, 1975; Dumitru et al., 2010; Morissani, 2006; Wakabayashi, 2015; Hopson et al., 2008; Shervais & Choi, 2012; Hamilton, 1969; Orme & Surpless, 2019). The Franciscan Complex transitions from east to west from coherently underplated, lawsonite-blueschist facies sedimentary and mafic rocks (Eastern Belt) (e.g., Jayko & Blake Jr, 1986; Wakabayashi & Dumitru, 2007; Dumitru et al., 2010; Schmidt & Platt, 2018) to a mélange unit consisting of high grade blocks within a low grade shaley matrix (Central Belt) (e.g., Cloos, 1983; Ukar, 2012; Platt, 2015) to a very low grade accretionary wedge (Coastal Belt) (e.g., Evitt & Pierce, 1975; Dumitru et al., 2013). The coherent blueschist facies lenses of the Eastern Belt underplated <30 km deep from 111-123 Ma (Dumitru et al., 2010; Apen et al., 2021). The Central Belt is a melange with a 75-95 Ma prehnite-pumpellyite facies shaley matrix encompassing older, higher grade blocks (Morissani, 2006; Cloos, 1983; Platt, 2015). The Coastal Belt consists of very low grade (zeolite facies) metasedimentary and rare metamafics imbricated to form a classic accretionary wedge during the Eocene to Miocene (Bachman, 1982; Dumitru et al., 2013). The Franciscan Eastern Belt (Fig. 1a) is in thrust contact (ca. 123 Ma) with the Western Klamath and Rattlesnake Creek terranes (Dumitru et al., 2010). A subunit of the Franciscan Eastern Belt, the South Fork Mountain Schist, is dominated by distal, hemipelagic protoliths (Dumitru et al., 2010; Schmidt & Platt, 2018) comparable to the CMS (Helper, 1986).

2.2 Condrey Mountain Schist (CMS)

The CMS records multiple generations of prograde ductile deformation in greenschist/epidote-amphibolite to epidote-blueschist facies rocks associated with subduction along a convergent margin (Fig. 2) (Helper, 1986; Tewksbury-Christle et al., 2021). The two main units (upper and lower CMS) are exposed through a structural window in the Klamaths due to regional doming, and the western limb of the dome is overturned from a primary east-dipping orientation (seen along Y-Y'-Y" cross section, Fig. 2b) (Helper, 1986). Uplift of onlap sequences constrains regional doming to the Neogene (Mortimer & Coleman, 1985), and low temperature thermochronology on plutons proximal to the CMS suggests some component of uplift in the Oligocene (Piotraschke et al., 2015). This regional-scale doming is roughly centered on the asymmetrical dome structure defined by the orientation of pervasive transposition foliations in the CMS (S_2, Fig. 2) (S_T in Helper, 1986; Mortimer & Coleman, 1985; Tewksbury-Christle et al., 2021).

The upper CMS is predominantly greenschist to epidote-amphibolite facies metavolcanic rocks with intercalated graphite phyllites metamorphosed at 0.3-0.5 GPa, 300-400°C (Helper, 1986). Concordant dioritic to tonalitic orthogneiss lenses crystallized at 170 ± 1 Ma (magmatic zircon U-Pb crystallization ages in Saleeby & Harper, 1993), suggesting that portions of the upper CMS are older than 170 Ma. Emplacement ages for the upper CMS are 156 ± 1 Ma, constrained by cross-cutting relationships with and cooling ages in the overlying Rattlesnake Creek terrane (Hacker et al., 1995; Saleeby & Harper, 1993). The pre-170 Ma upper unit protolith age constraint places these rocks within the age range of Western Hayfork arc volcanics, and emplacement beneath the base of the Rattlesnake Creek terrane is roughly coeval with motion on the Orleans fault.

High angle, possibly late stage faults juxtapose the lower CMS against the upper CMS, though lower angle faults marked by small metaserpentinite and metagabbro bodies are locally preserved (Helper, 1986). In contrast to the upper CMS, the lower CMS consists primarily of hemipelagic or pelagic sediments with m- to km-scale mafic and serpentinized ultramafic intercalated lenses, all metamorphosed to epidote-blueschist facies (0.7-1.1 GPa, 400-450°C) to form graphite mica schist, epidote blueschist, and metaserpentinite, respectively (Helper, 1986; Tewksbury-Christle et al., 2021). Although the sediments entered the subduction zone on the downgoing plate, geochemical evidence suggests that tectonic erosion of the overriding plate sourced the ultramafic and some of the mafic lenses (Tewksbury-Christle et al., 2021).

Tewksbury-Christle et al. (2021) further characterized the fossil subduction interface, prograde deformation, and underplating processes that assembled the lower CMS rocks. These rocks record multiple generations of prograde ductile deformation. A pervasive transposition foliation that defines the CMS dome structure (S_2, Fig. 2) is coherently developed across heterogeneous lithologies, suggesting assembly of the tectonically eroded material and incoming sediments prior to coherent deformation and subsequent underplating. Strain localization proximal to km-scale mafic + ultramafic lenses resulted in a phase of locally developed overprinting structures (S_3 and F_3, localization marked in Fig. 2b). These structures broadly divide the lower CMS into three main underplated packages. Thin incoming sediment packages and rare m-scale mafic + ultramafic lenses underplated and were entrained during ongoing underplating and deformation. Introduction of km-scale mafic + ultramafic lenses allowed for strain localization, abandonment of the previously underplated package, and down-stepping of the subduction interface. Subsequent underplating initiated below the ductile thrust zone. Multiple underplating phases suggest a possible protracted history that could provide insights into evolution of this portion of the western North American margin.

Because of limited age data, however, regional correlations amongst the subduction record of the CMS, other Klamath terranes, and the Franciscan Complex are currently poorly constrained. Extant CMS dates are consistent with regional correlations, in whole or in part, between the CMS and either 1) the Western Klamath terrane (e.g., Klein, 1975; Saleeby & Harper, 1993), 2) the Franciscan Eastern Belt (e.g., Brown & Blake, 1987; Chapman et al., 2021) or 3) none of the Klamath terranes or Franciscan Complex (e.g., Hill, 1985). Correlation to the Western Klamath terrane is based on lithologic similarities to the Galice Formation within the Western Klamath terrane and regional relationships, which show the CMS and Western Klamath terrane are both structurally beneath and in fault contact with the Rattlesnake Creek terrane (Fig. 1b and c) (Saleeby & Harper, 1993). Comparable emplacement timing of the upper CMS and the Western Klamaths further supports this correlation. Previously cited ages for the lower CMS, however, include white mica K-Ar cooling ages (118 ± 2 Ma[1] and 128 ± 2 Ma[2]), a sodic amphibole K-Ar cooling age (127 ± 6 Ma[2]) (Coleman et al. (1983)[1];Helper (1986)[2]), and detrital zircon maximum depositional ages (MDAs, 143-129 Ma) (Chapman et al., 2021), overlapping with, or closely predating, emplacement of the Franciscan Eastern Belt ca. 123 Ma, suggesting that the lower CMS might instead be a down-dip continuation of the Franciscan Eastern Belt (c.f., Brown & Blake, 1987) and that the Western Klamath terrane either correlates with the upper CMS only or pinches out between the two (Fig. 1c). A third, largely unaddressed alternative, is that the lower CMS correlates with neither the Western Klamath terrane nor the Franciscan Eastern Belt. Although Hill (1985) offered this alternative, he did so on the basis of an upper CMS occurrence west of the window along the Klamath River, treating the upper and lower CMS as a single terrane. In so doing, he concluded that the Condrey Mountain Terrane pre-dated formation and assembly of the Western Klamath Terrane and was emplaced prior to it, after 162 and before 150 Ma (Fig. 1c).

In addition to helping regional correlations, improved age data can help better constrain global mass and volatile recycling estimates. Modern tectonically erosive margins are estimated to contribute significantly to supplying continental material and carbon to the upper mantle at 65% and 30% of the total, respectively (Clift, 2017; Clift et al., 2009). These budgets, however, assume no underplating processes in erosive margins. Tewksbury-Christle et al. (2021) demonstrated that the lower CMS subducted along a margin undergoing shallow tectonic erosion and deep underplating that preserved an estimated 10-60% of the incoming sediment from being recycled into the upper mantle. The significant uncertainty in their estimates comes from limited age constraints that can be improved with additional depositional and metamorphic ages for the lower CMS.

3 Methods

3.1 Dating lower CMS crystallization and deposition

Magmatic zircon U-Pb geochronology. U-Pb zircon dates from the Scraggy Mountain epidote blueschist lens (Fig. 2a) were collected by Helper and N. Walker at University of Austin's TIMS laboratory (1988), but these legacy data were previously unpublished (data, standards, and detailed methods in Dataset S1).

Detrital zircon U-Pb geochronology. We sampled a transect across the structural thickness of the lower CMS (Fig. 2) to map depositional age variation with structural depth. Samples were prepared by mechanical crushing and density and magnetic separation. Zircons were sprinkle mounted on double-sided tape and unpolished zircon grains were U-Pb dated using depth profiling laser ablation technique (e.g., Marsh & Stockli, 2015) at the University of Texas at Austin's geochronology lab (UTChron). Depth-profile analysis allows for spatial recovery of multiple zircon age domains during progressive ablation. The LA-ICP-MS system, which consists of an Analyte G.2 193 nm Excimer laser ablation system with a Helex sample cell attached to an Element2 HR-ICP-MS. For each U-Pb analysis, a 30 μm laser spot with a nominal energy of 4 mJ, an average fluence of 1.98 J/cm^2, and a pulse rate of 10 Hz was used to ablate zircons at a depth of 15 μm. This allowed for a <0.5 µm depth resolution of different age domains. For this study, GJ1 (Jackson et al., 2004) was the primary standard to correct for downhole, elemental, and isotopic fractionation, and two secondary standards (Plešovice, Sláma et al. (2008) and 91500, Wiedenbeck et al. (1995)) were analyzed to monitor data quality. Data reduction was performed using the Iolite (Paton et al., 2010) and VisualAge data reduction scheme (Petrus & Kamber, 2012) within the WaveMetric IgorPro software package. Best zircon U-Pb ages were obtain based on a zircon's age with respect to 850 Ma and discordance between ^{206}Pb/^{238}U and ^{207}Pb/^{235}U ages. ^{206}Pb/^{238}U ages were used for grains younger than 850 Ma, including two-sigma internal error, while ^{207}Pb/^{206}Pb ages were used for grains older than 850 Ma. Zircon ages were eliminated if grains contained greater than 10% analytical error, the ^{206}Pb/^{238}U age error was greater than 10%, or the ^{207}Pb/^{235}U age errors was greater than 10% and had greater than 10% discordance.

For detrital provenance and maximum depositional age determinations, we analyzed 120+ zircon grains per sample to ensure the capture of any age component >5% (Vermeesch, 2004). We calculated maximum depositional age (MDA) for each sample as the youngest single grain (YSG), youngest 2+ grains that overlap at 1σ (YC1σ), and youngest 3+ grains that overlap at 2σ (YC2σ) (Dickinson & Gehrels, 2009) after omitting grains with ^{206}Pb/^{238}U discordance and/or error >10% (Dataset S2). We report the pooled 1σ and number of grains for each MDA. We present YC1σ as the best constraint of lower CMS depositional ages. YSG is more likely than the other methods to result in an MDA younger than the true depositional age, and YC2σ is more likely to overestimate the depositional age (Dickinson & Gehrels, 2009).

Depth profile LA-ICP-MS analysis on detrital zircons allows for dating of thin metamorphic or igneous zircon rims (e.g., Poulaki et al., 2021). Where rims are present and measurable, we report an age for both the zircon rims and cores and use the word 'rim' throughout to denote presence of overgrowths without interpretation (e.g., metamorphic or igneous growth). In addition, we employed split-stream LA-ICP-MS analysis, using two Element2 instruments, to simultaneously acquire U-Pb dates, trace element, and rare earth element (REE) data over depth profiles for selected samples (Section 4.1). We also gathered cathodoluminescence (CL) images on selected depth-profiled grains using a Deben Centaurus panchromatic CL system on the JEOL JSM-6390 LA scanning electron microscope (SEM) at ETH Zurich's Electron Microscopy Lab and a Gatan MiniCL on the FEI Quanta 200F SEM at ETH Zurich's ScopeM.

3.2 Dating lower CMS metamorphism

K-Ar and Rb-Sr geochronology. K-Ar and Rb-Sr dates were collected at the University of Texas at Austin by F. McDowell (1988-89) and Helper (1987-89), respectively, but these legacy data, similar to the U-Pb dates on magmatic zircons in Section 3.1, were previously unpublished. K-Ar dates presented below and in Dataset S3 are for white mica. Rb-Sr multi-mineral isochrons are defined by apatite-whole rock-white mica, unless otherwise noted (Dataset S4 and Fig. S1). Both K-Ar and Rb-Sr closure temperatures (350-450°C and 550°C, respectively) (e.g., Jäger, 1979; Ruffet et al., 1997; Scaillet, 1998) are near to or higher than the lower CMS peak temperatures (Helper, 1986; Tewksbury-Christle et al., 2021), so these geochronometers constrain either timing of metamorphism or coeval metamorphism/cooling.

To better interpret spatial variations in depositional and/or metamorphic ages, we characterized peak temperatures using graphite crystallinity, where jumps in temperature might be indicative of cryptic structures that would affect the spatial distribution of ages. Graphite Raman spectra vary systematically with peak temperature (330-650°C) and are not sensitive to pressure or retrogression (e.g., Beyssac et al., 2002). We analyzed samples from a transect across the lower CMS structural thickness (Fig. 2) on ETH Zurich's DILOR Labram micro-Raman spectrometer, used Igor Pro for baseline correction and peak fitting, and applied Beyssac et al. (2002)'s temperature calibration. Reported temperatures average results from 10 analyses per sample (average peak fits and temperatures in Dataset S5), and we report the standard error.

Three detrital zircon samples (stars, Fig. 2) exhibit complex spatial relationships with respect to their MDAs. To aid in interpretation of these results, we collected graphite crystallinity data on these samples, as well as Si content in two generations of white mica growth (D_1 and D_2, Tewksbury-Christle et al., 2021). Although the CMS lacks the limiting assemblage needed to calculate an absolute pressure using the Si-in-phengite geobarometer (Massonne & Schreyer, 1987), Si concentrations can constrain relative pressures amongst these samples. We measured Si on the ETH Zurich's JEOL JXA-8230 Electron Probe Microanalyser and calculated Si p.f.u. assuming all ferrous Fe (calibration standards and calculated Si per formula unit detailed in Dataset S6).

4 Results

4.1 Lower CMS crystallization and deposition ages

Magmatic zircons from the Scraggy Mountain epidote blueschist lens (Fig. 2a) date to 169 ± 2 (magmatic zircon TIMS U-Pb). This age is comparable to the Western Hayfork arc in the Klamaths.

Detrital zircon U-Pb ages from from the lower CMS are characterized by a large component of Western Hayfork arc ages, but the youngest zircon components, and hence the MDAs, significantly postdate the age of crystallization of the Scraggy Mountain lens. Detrital zircon spectra plotted as Kernel Density Estimations (KDEs, Figures S2 and S3 with color bins that follow Sharman et al. (2015)) are dominated by <500 Ma grains with only minor older components of up to 3.0 Ga. The bulk of the detrital zircons yield dates <170 Ma with peaks between 145 Ma and 155 Ma, coeval with the Rogue-Chetco arc in the Klamaths (Yule et al., 2006). The oldest MDA using any method is 155 ± 3 Ma, but 8 of the 11 samples have an MDA younger than 150 Ma, regardless of the method used. Employing YC1σ method, MDAs range from 135-150 Ma with limited correlation between age discontinuities and mapped structures (Figs. 3 and 4). CT-CMW36, for example, yields a younger MDA (135 ± 1 Ma) than the samples both structurally above and below it (149 ± 1 Ma and 153 ± 2 Ma, respectively), but all three are within the same thrust-bounded package (Tewksbury-Christle et al., 2021). Grains from CT-CMW36 have sectoral or poorly developed zonation, whereas grains from other samples have clear oscillatory zonation in the cores (CL images in Fig. 5 and S4).

Zircon rims show a range of behavior with respect to trace elements and REEs. Cores primarily have Th/U > 0.1 (Fig. 5), consistent with igneous zircons (Hoskin & Schaltegger, 2003; Rubatto, 2017; Yakymchuk et al., 2018) or recrystallized igneous zircon (e.g., Poulaki et al., 2021). Rims, however, have a wide range of Th/U values, with populations of rims with Th/U > 0.1 that both pre- and postdate the MDA. CL images show that some grains with low Th/U rims have irregular rims that cut oscillatory zoning in the cores (e.g., CT-CMW42 and CT-CMW55, Fig. 5), while others have more conformable planar boundaries between a bright core and dark rims (CT-CMW35, Fig. 5). Grains with high Th/U rims have both planar oscillatory zoning (CT-CMW55) and more diffuse irregular boundaries (CT-CMW42). Additional CL images are presented in Fig. S4. For the two samples with REE analyses (CT-CMW36 and CT-CMW53), Ce/Ce* versus Sm/La show that most single ages and cores plot in the igneous field (e.g., Hoskin, 2005), but some plot in the metamorphic field or between the two fields, and a similar spread occurs in the zircon rims (Fig. 6). Th/U ratios appear to be poorly correlated to Ce/Ce* versus Sm/La, with low Th/U rims plotting predominantly in or close to the igneous field (Fig. S5).

4.2 Lower CMS metamorphic ages, peak temperatures, and relative pressures

Multi-mineral isochron Rb-Sr dates and white mica K-Ar dates postdate the MDAs (Fig. 4a). Rb-Sr dates range from 119-132 Ma and average 124 ± 7 Ma. K-Ar dates range from 124-133 Ma and average 128 ± 2 Ma. These dates have a wide range but young broadly downwards.

Peak temperatures from graphite crystallinity show little variation across the structural thickness. The temperatures average 460 ± 10°C with a minor inverted metamorphic gradient (approximately 1.5°C/km). Temperature variations do not correlate with mapped structures. Peak temperatures from graphite crystallinity (Fig. 4b) and relative pressures from Si-in-Phengite (Fig. S6) are not significantly different amongst the top three samples collected for detrital zircon geochronology. Pressures from multiple generations of white mica growth are also not significantly different from each other.

5 Synthesis of data to determine timing of Lower CMS emplacement

5.1 Interpretations of calculated MDAs

All MDAs are 135-153 Ma with complex spatial behavior across increasing structural depth, where MDA discontinuities are not always correlated with inferred and/or observed structures. MDA discontinuities of ca. 5-18 Ma occur within packages imbricated by ductile thrusts. Out of sequence thrusting or large scale folding could explain the repetition of the ca. 135 Ma MDA towards the top of the structural package (CT-CMW36) that results in the largest MDA discontinuity (Fig. 4), but structural observations do not support either explanation. We observed no evidence of folding at wavelengths comparable to the structural thickness, brittle faulting between these samples, or strain localization that could be indicative of ductile thrusting (Tewksbury-Christle

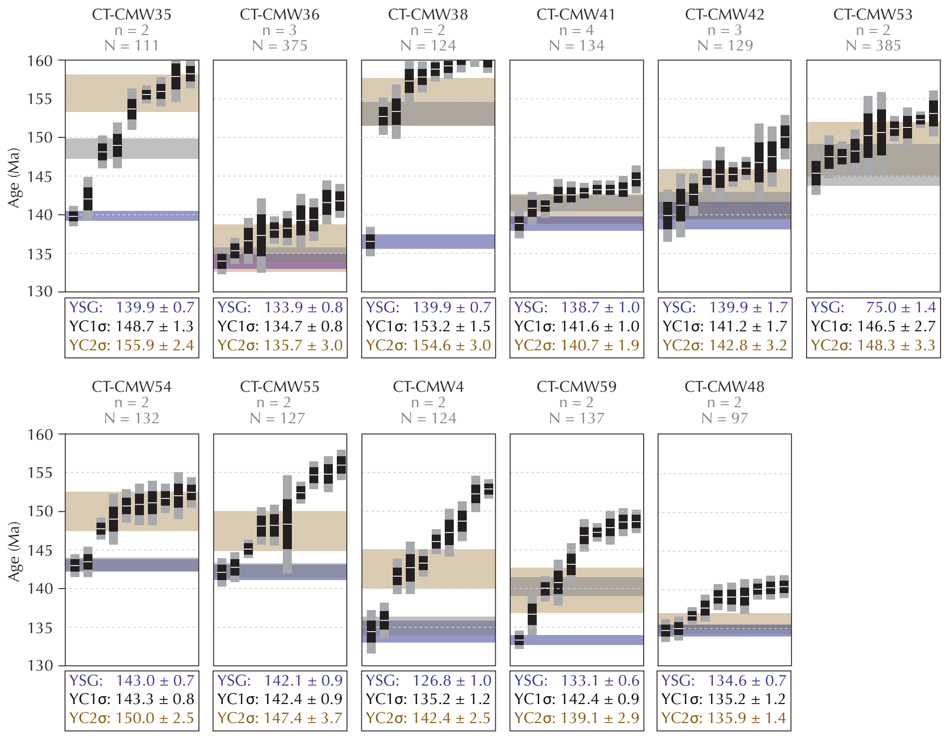

Figure 3. Age of the youngest ten grains in each sample ($\pm 1\sigma$ in black, $\pm 2\sigma$ in gray), with increasing structural depth from left to right, top to bottom. Colored bars mark the calculated MDA for the three different methods: youngest single grain (YSG; violet), youngest two or more grains that overlap at 1σ (YC1σ; gray), and youngest three or more grains that overlap at 2σ (YC2σ; brown). N is the number of concordant grains out of the 120+ analyzed. n is the number of grains used to calculate the MDA using YC1σ. CT-CMW36 and CT-CMW53 were also analyzed for REEs, resulting in a larger number of total grains.

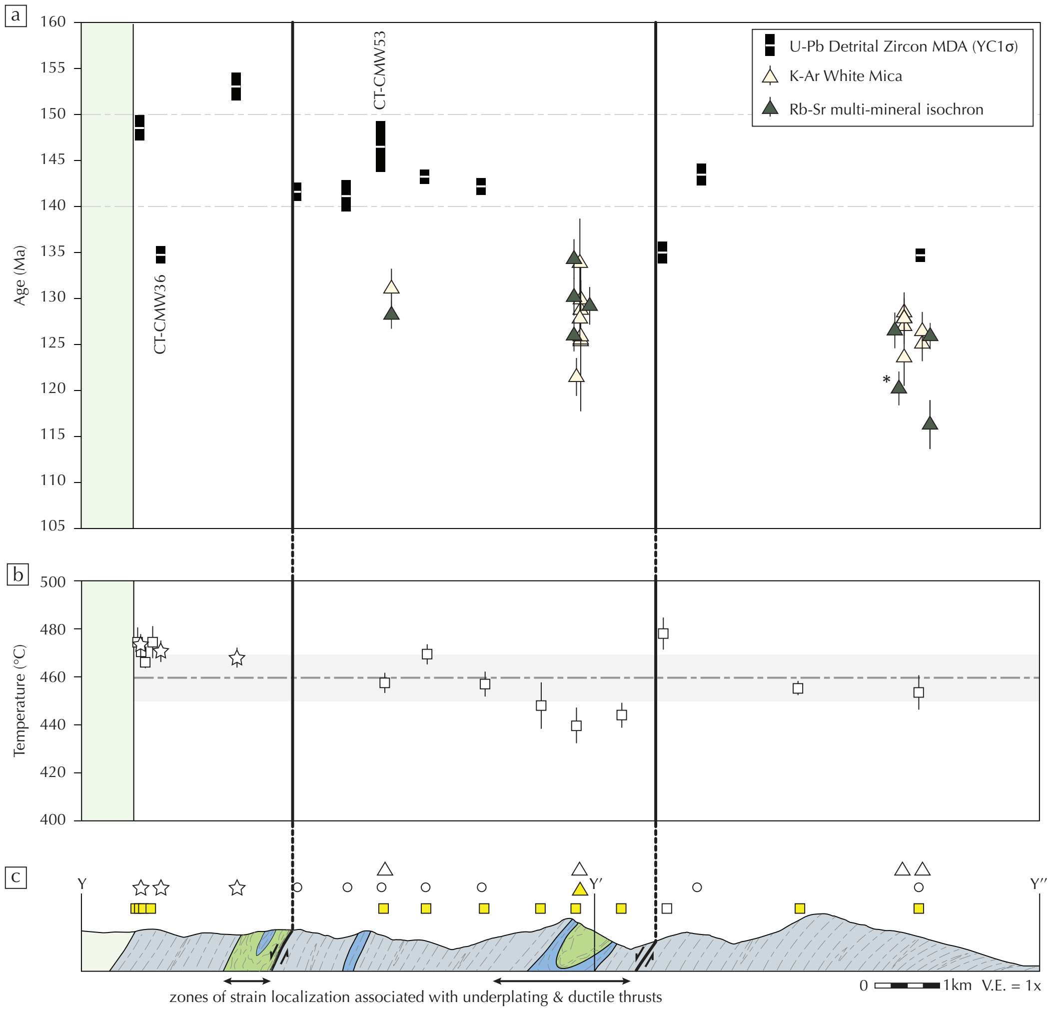

Figure 4. a) Variation of MDAs ($\pm 1\sigma$) and metamorphic dates across the lower CMS structural thickness. Sample locations follow Fig. 2, and black lines mark ductile thrusts recognized by Tewksbury-Christle et al. (2021). Sample marked with (*) was calculated using a titanite-whole rock-phengite isochron. All others use an apatite-whole rock-phengite isochron. MDA discontinuities do not typically correlate with mapped ductile thrusts. Metamorphic ages young broadly downward and closely postdate the youngest MDAs. REE analyses on labeled samples presented in Fig. 6a-b. b) Peak temperatures from graphite crystallinity show limited variation with structural depth. c) Sample locations projected onto the Y-Y'-Y" cross section line in Fig. 2. Symbols in (b) and (c) follow Fig. 2.

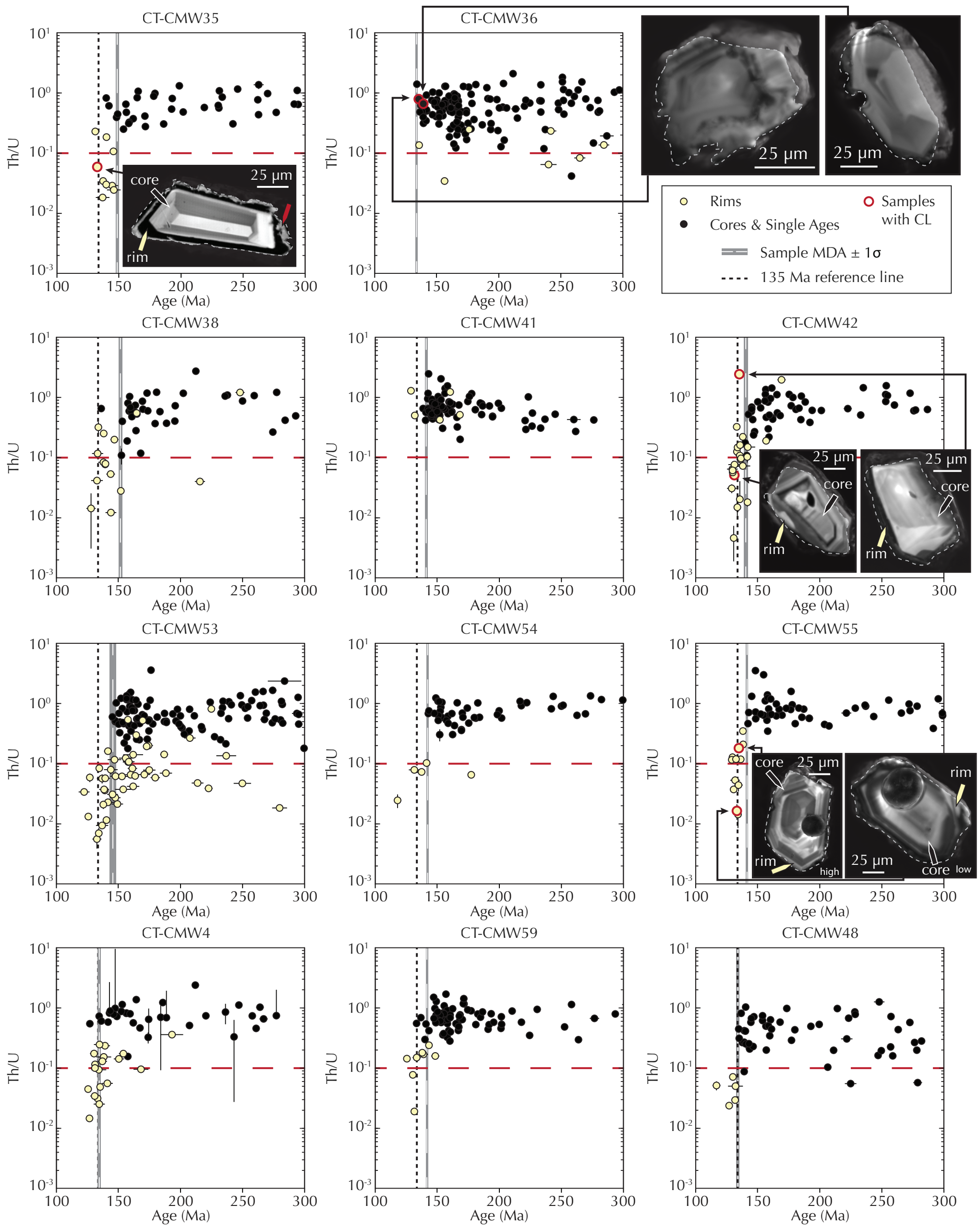

Figure 5. Th/U variations by sample for rims and cores/single ages. Structural depth of the samples increases from left to right, top to bottom. Where not shown, error bars are smaller than symbol size. Most samples show a slight decrease in Th/U when considering both cores and rims approximately coeval with the calculated MDA (gray bar showing $\pm 1\sigma$). Most rims, cores, and single ages are older than 135 Ma (dashed reference line), but younger low Th/U rims are present throughout the structural package. Example CL insets from CT-CMW35, CT-CMW42, and CT-CMW55 show cores with oscillatory zoning and predominantly irregular rims. Grains from CT-CMW36 have sector or poorly developed zoning. Yellow and black arrows mark rims and cores, respectively, and dashed gray lines outline the polished surface of the zircons. Bright irregular zones at the grain margins in CT-CMW35 are tape residue (red arrow). Additional CL images from these samples are in Fig. S4.

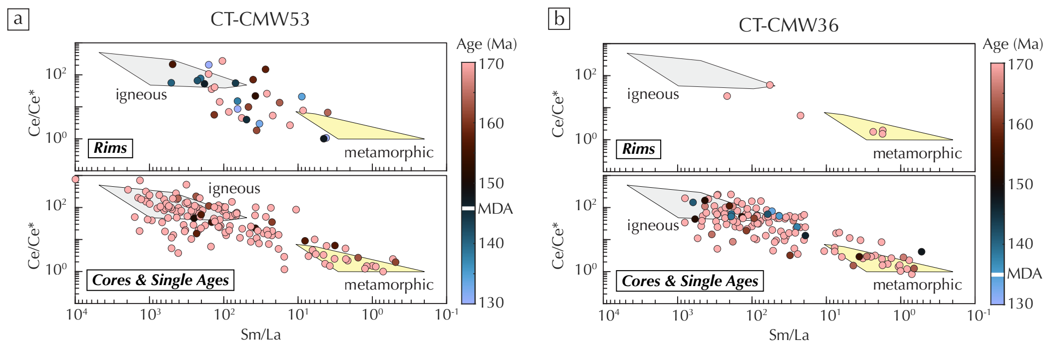

Figure 6. REE variations in CT-CMW53 (a) and CT-CMW36 (b) (data available in Dataset S7). Fields after Hoskin (2005). The calculated MDA is plotted as a white line in the color bar. Rims in CT-CMW53 show a range of affinity, whereas cores/single ages plot predominantly in or near the igneous field. Rare rims in CT-CMW36 plot in the metamorphic field or in the area between the two fields.

et al., 2021). Peak temperatures are also consistent across the structural thickness, with no significant variations in temperature correlated with MDA discontinuities. Relative pressures across the three topmost samples are comparable amongst the samples and deformation phases. Together, these data suggest that the lower CMS protoliths were subducted and assembled along the same prograde path. In the case of later juxtaposition via cryptic thrusts, folding, or melange mixing, we would expect samples with different depositional ages to have different pressure and/or temperature histories.

We can interpret the relatively anomalously young CT-CMW36 MDA (Fig. 4) as either representative of the true maximum depositional age or as younger metamorphic zircon recrystallization and overprinting. Peak temperatures constrained by graphite crystallinity (460 ± 10°C) are lower than temperatures needed to form new zircon grains (≥ 580°C, Watson et al., 2006). Graphite crystallinity is not sensitive to retrogression, and the graphitic mica schist records prograde deformation across the phengite + graphite + quartz + chlorite ± albite assemblage as indicated by both temperature constraints and Si-in-phengite compositions. Young dates in CT-CMW36 are associated with high Th/U more characteristic of magmatic zircons and with igneous affinity Ce/Ce* versus Sm/La. Metamorphic zircons can have high Th/U (Hoskin & Schaltegger, 2003; Rubatto, 2017; Yakymchuk et al., 2018; Poulaki et al., 2021), however, and all REE analyses from these samples have a range of affinities. Rims in CT-CMW42, for example, appear to be metamorphic based on the irregular rims cross-cutting oscillatory zonation (yellow arrows, Fig. 5) but have both high and low Th/U. Furthermore, internal zonation is poorly developed in the CL images of CT-CMW36 and morphologically different from the internal structure of zircons from other samples (Fig. 5 and S4), supporting a possible metamorphic origin. Tomaschek et al. (2003) proposed topotactic fluid-assisted dissolution and replacement of igneous zircons from metabasites in Syros, Greece, that reset the U-Pb ages during prograde metamorphism at 480°C and 1.6 GPa. Although still higher grade than the lower CMS, this temperature is much lower than zircon crystallization temperatures and might explain the internal morphology of the CT-CMW36 zircons. Poulaki et al. (2021) demonstrated similar conditions in the Cycladic subduction complex for both fluid-absent and fluid-assisted metamorphic zircon recrystallization that resulted in REE signatures that were partially inherited from the crystallized zircon core.

Because these zircon trace element data are non-diagnostic, we present two different possible interpretations of lower CMS deposition and emplacement. Regardless of how we interpret CT-CMW36, the MDAs of the other samples still bracket the oldest possible deposition of the lower CMS at ≤153 Ma, with the majority of samples <150 Ma (Fig. 3 and 4). These results definitively preclude correlation with the Western Klamath terrane. The interpretation of CT-CMW36 simply determines the duration of deposition of the lower CMS. The possible scenarios for CT-CM36 are:

1. *The MDA is representative of the lower CMS true maximum depositional age.* In the absence of structural repetition, or melange mixing and assuming no growth of metamorphic zircons, this complex spatial behavior across increasing structural depth (illustrated in Fig. 4) is best explained as true maximum depositional ages, where samples with MDAs older than ca. 135 Ma are missing the youngest population of detrital zircons. The lower CMS graphite schist protolith was hemipelagic (Helper, 1986), indicative of distal, deep water deposition with possible concomitant heterogeneous distributions of zircon populations in protolith sediment. For example, 24% of the grains in CT-CMW41 are <150 Ma, compared to ≤10% for the majority of the other samples. If the youngest population is not present in all samples due to heterogeneous source input, the MDA could overestimate the true depositional age but still bracket the oldest possible deposition. In this circumstance, we would therefore interpret the youngest MDAs (ca. 135 Ma) as best constraining deposition of the lower CMS, with subduction and emplacement post-dating 135 Ma.
   If the CT-CMW36 MDA is the true depositional age, zircon rims from the other samples can be interpreted in multiple ways. Zircon rim ages predominantly post-date the MDA in individual samples, but many predate 135 Ma (dashed lines, Fig. 5). In CL, the morphology of these rims appears to be consistent with both igneous (CT-CMW35, despite low Th/U) and metamorphic (CT-CMW42, despite low and high Th/U) overgrowths. The morphology, therefore, appears to have limited correlation to Th/U values. REE analyses are similarly non-diagnostic, showing a range of affinities in Ce/Ce* versus Sm/La that are commonly contradictory to Th/U (e.g., rims with igneous affinity but low Th/U, Fig. S5). Although igneous rims are rarely <0.1 (Hoskin & Schaltegger, 2003; Rubatto, 2017; Yakymchuk et al., 2018), magmatic zircons grown in fractionated magmas can have low Th/U (Kirkland et al., 2015), consistent with the tonalite-trondhjemite-granodiorite and granodiorite suites that characterized late stage plutonic activity in the Klamaths (Allen & Barnes, 2006). Recrystallized rims formed during metamorphism, however, may inherit the REE and Th/U signature of the cores (e.g., Poulaki et al., 2021), which might account for the range of REE affinities. If we interpret the rims as igneous, then our MDAs overestimate the true depositional age. If we interpret the rims as metamorphic, then many of the dated zircons would need to be subducted prior to the minimum depositional age of the lower CMS at 135 Ma. Because the lower CMS subducted along a tectonically erosive margin (Tewksbury-Christle et al., 2021), these metamorphic rims could be the record of older, previously underplated blocks that were stripped off during subduction erosion, intercalated into the younger incoming sediment, ductilely deformed along the prograde path, and subsequently underplated at depth after 135 Ma. Given the CL imagery, the best explanation is likely a mix of the two cases, where some zircons have igneous rims that would result in a lower MDA for the sample and others have metamorphic rims that would necessitate intercalation of older sediments already in the subduction interface.
2. *Young CT-CMW36 zircon cores are metamorphic.* In this case, the young CT-CMW36 zircon ages need to be excluded from the calculated MDA, and individual MDAs of other samples are representative of their true maximum depositional ages. The lower CMS maximum depositional ages, therefore, would young broadly downwards from 149 to 135 Ma (Fig. 3), and older MDAs towards the bottom of the structural package could be due to heterogeneous zircon provenance, as discussed above.

This younging downward pattern is consistent with five MDAs discussed in Chapman et al. (2021). Age discontinuities spatially correlated with ductile thrusts (black lines, Fig. 4) could represent brief periods with no underplating during strain localization to the km-scale mafic+ultramafic lenses that facilitated assembly of the lower CMS (Tewksbury-Christle et al., 2021).

5.2 Timing of lower CMS emplacement and underplating

Metamorphic white mica K-Ar (Dataset S3) and multi-mineral-isochron Rb-Sr dates (Dataset S4) place constraints on subduction and emplacement of the lower CMS, independent of the detrital zircon ages. By this measure, metamorphism in the lower CMS ranged from 119-133 Ma with a downward-younging trend, closely post-dating the youngest MDAs (<5 Ma; Fig. 3 and 4). This age range is consistent with cessation of arc magmatism west of or in the vicinity of the CMS window (Allen & Barnes, 2006). Before ca. 135 Ma, active plutonism was either outboard and west of the CMS or fell along approximately the same longitude, so older lower CMS emplacement would have required underplating below an arc or in the backarc. After ca. 135 Ma, there is no active arc signature within the Klamaths (Allen & Barnes, 2006). Remnants of the arc active during lower CMS emplacement are presumably buried under the Cretaceous onlap sequences to the east, along the structural trend of the Sierra Nevada batholith.

6 Implications

6.1 Implications for CMS terrane affinity within the Klamaths and Franciscan

Our new geochronologic results preclude correlation of the lower CMS with either the Western Klamath terrane or the South Fork Mountain Schist (Fig. 7a-b). The lower CMS depositional ages are younger than the Western Klamath terrane (Fig. 7c). Even if we consider the most conservative estimate of MDA (YC2σ), the majority of samples were deposited after 150 Ma and thus postdate deposition of the Western Klamath terrane (Frost et al., 2006; Macdonald et al., 2006). Furthermore, onset of metamorphism in the lower CMS predates and overlaps with subduction and metamorphism of the South Fork Mountain Schist (Dumitru et al., 2010).

The transition of the western North American margin from outboard subduction and accretion of fringing island arcs to an along-strike coherent Andean-style margin occurred during the early Franciscan history. The Klamaths record sporadic terrane accretion, whereas the Franciscan Complex preserves development of an accretionary wedge at a well-developed, Andean-style subduction margin. Based on our new geochronologic constraints, the lower CMS fits into the temporal gap between the end of Klamath-style subduction and the onset of accretionary tectonics in the Franciscan, with underplating of the lower CMS starting before the earliest coherent underplating in the Franciscan and then continuing during underplating of the South Fork Mountain Schist.

6.2 The CMS as a record of earliest Franciscan underplating

Reconstructions of primary subduction margins from the Klamath terranes are particularly challenging given the complex structural relationships of multiple overprinting accretion events. The aggregated Klamath terranes preserve evidence of multiple fringing subduction margins that were subsequently stacked along the North American margin. Imbricated arc and basinal terranes that sandwich rare subduction complexes (e.g., Snoke & Barnes, 2006, and references therein) collectively suggest the existence of four fringing subduction margins affiliated with, from east to west: 1) an unidentified continental North American arc, 2) the Redding arc and related terranes (Trinity and Yreka), 3) the North Fork arc, and 4) the Rattlesnake Creek-Western Hayfork (RSC-WHF) arc

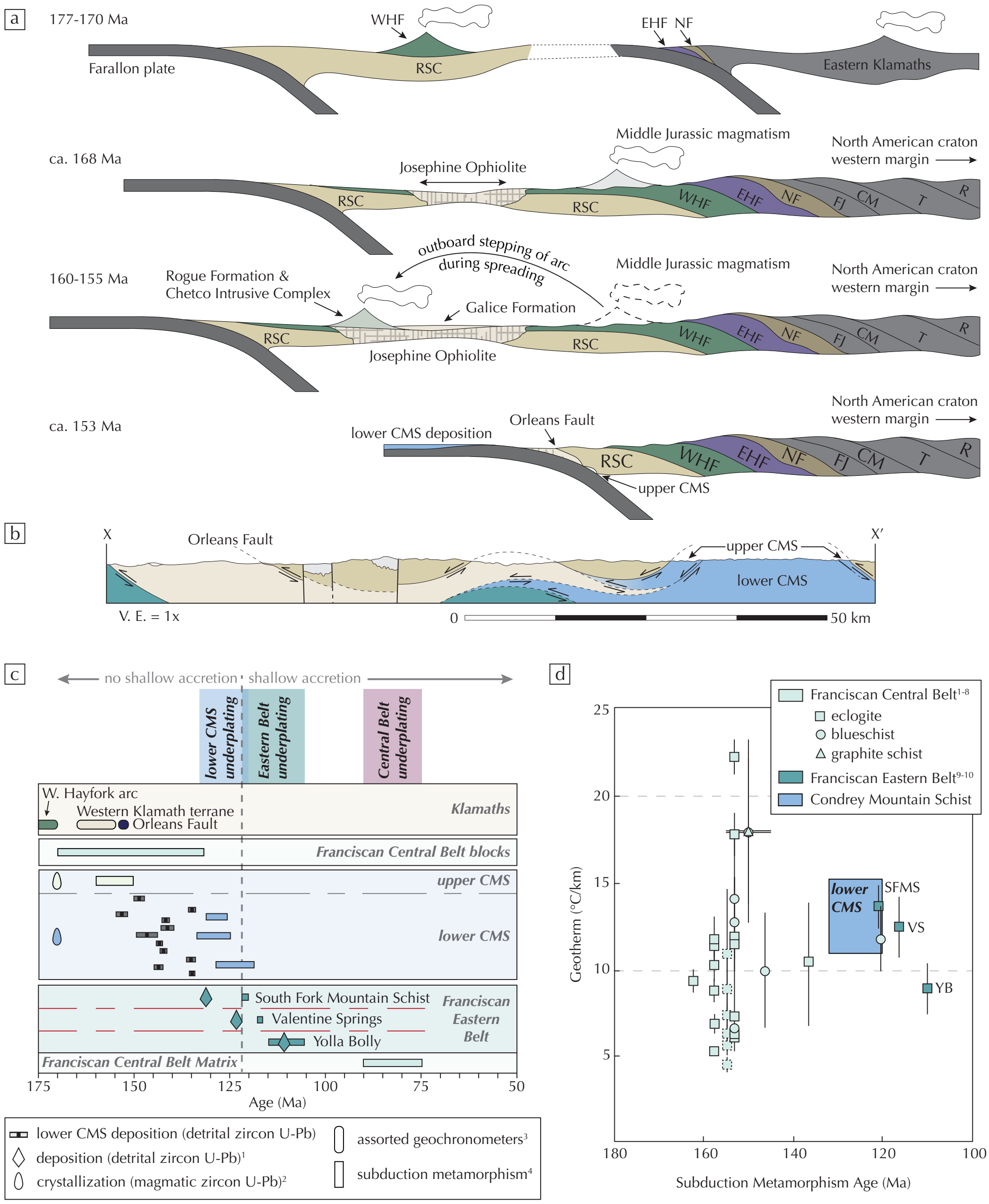

Figure 7. a) Schematic cross sections showing evolution of the Klamath margin. The Klamaths preserve evidence of a single subduction margin outboard of the Rattlesnake Creek and Western Klamath terranes from the Late Triassic to the Early Cretaceous. Colors and abbreviations follow legend in Fig. 1. b) Cross-section along X-X' in Fig. 1 showing the correlation that is most consistent with the data presented in this study. c) Timeline of Klamath and Franciscan tectonics including geochronologic constraints from this study. All lower CMS ages are presented in this study. Others are sourced as follows: [1]Dumitru et al. (2010); [2]Saleeby and Harper (1993); [3]Snoke and Barnes (2006); [4]for the upper CMS: Hacker et al. (1995); Saleeby and Harper (1993), for the Franciscan: Dumitru et al. (2010); Morissani (2006). The dashed line marks onset of accretionary subduction in the Franciscan (c.f., Dumitru et al., 2010). d) Geothermal evolution of the Franciscan margin through time, constrained by Franciscan P-T estimates from: [1]Cooper et al. (2011); [2]Page et al. (2007); [3]Massonne (1995); [4]Krogh Ravna and Terry (2004);[5]Krogh et al. (1994); [6]Tsujimori et al. (2006); [7]Wakabayashi (1990); [8]Ukar and Cloos (2016); [9]Dumitru et al. (2010); [10]Schmidt and Platt (2020). All blocks from the same location are plotted with ages from Cooper et al. (2011). Where ages are not available, dashed symbols are plotted against an average age for block metamorphism from Cooper et al. (2011). SFMS: South Fork Mountain Schist, VS: Valentine Springs, YB: Yolla Bolly.

(Saleeby, 1990; Wright & Wyld, 1994; Snoke & Barnes, 2006). Based on our data from the lower CMS, coupled with regional relationships, we hypothesize that the RSC-WHF arc was built above a proto-Franciscan margin, based on the following lines of evidence:

1. The Franciscan Eastern Belt is in thrust contact with the Western Klamath terrane (Fig. 1a). Although the Eastern Belt post-dates the Western Klamath terrane, the Eastern Belt represents underplated material subducted on the downgoing Farallon slab along the Franciscan margin (e.g., Dumitru et al., 2010). The Western Klamath terrane comprises arc- and forearc-related units (e.g., Snoke & Barnes, 2006). The simplest interpretation would place a subduction margin between these two units, which would have been the Franciscan margin at the time of Eastern Belt subduction (≤123 Ma).
2. The remains of a different trench do not exist between the RSC-WHF arc and the Franciscan Eastern belt. If Franciscan subduction initiated along a new trench outboard of the RSC-WHF margin, juxtaposing the Franciscan Eastern Belt (downgoing slab of this Franciscan margin) against the Western Klamath terrane (which is in the overriding plate of the RSC-WHF margin) would require removal of: 1) any subduction complex material affiliated with the RSC-WHF margin, 2) the intervening downgoing plate material between the RSC-WHF margin and the Franciscan margin, and 3) backarc and forearc deposits, as well as arc rocks, affiliated with the Franciscan margin. We do not see evidence of these units in the Klamaths.
3. The RSC is an ophiolitic mélange overlain by volcanic cover that formed the basement for the WHF arc (Wright & Wyld, 1994; Frost et al., 2006). RSC-WHF volcanics and plutons date from the late Triassic to ca. 170 Ma (Snoke & Barnes, 2006) (Fig. 7a). After imbrication of the Klamath terranes, the Wilson Point thrust between the Eastern and Western Hayfork terranes is cut by a suite of Middle to Late Jurassic plutons (168-152 Ma) that indicate construction of a new arc on top of the juxtaposed North Fork, Eastern and Western Hayfork, and RSC terranes (Fig. 1 and 7a) (Saleeby, 1990; Wright & Wyld, 1994; Snoke & Barnes, 2006). These plutons are typically interpreted to represent continued volcanism in the RSC-WHF arc, where suturing of the upper plate terranes has no effect on continued subduction along the RSC-WHF margin, except to change the configuration of the overriding plate (e.g., Wright & Wyld, 1994).
   Subsequent forearc spreading forming the Josephine Ophiolite (ca. 165-161 Ma) and associated basinal deposits (158-151 Ma) (Saleeby & Harper, 1993; Hacker et al., 1995; Snoke & Barnes, 2006; Yule et al., 2006; Surpless et al., 2023), and forearc basin closure (ca. 153-150 Ma) (Snoke & Barnes, 2006, and references therein) shuffled the relative location of the trench with respect to the RSC-WHF arc, but did not change subduction along the margin (Fig. 7a). Ongoing volcanism in the Rogue-Chetco arc (Yule et al., 2006; Garcia, 1982) suggests ongoing subduction along the RSC-WHF margin through the Late Jurassic.

Given these different lines of evidence, we propose that Late Triassic onset of volcanism in the RSC-WHF arc is indicative of proto-Franciscan subduction initiation, which occurred earlier in the north, outboard of the Klamaths, than in the south. The margin between the Western Klamath terrane and the Franciscan Eastern Belt was the Franciscan subduction margin by the Early Cretaceous. There is no evidence that a secondary margin existed between the Franciscan and the rest of the Klamaths, suggesting that the Franciscan margin is the same as the RSC-WHF margin, thus designating the RSC-WHF margin the proto-Franciscan margin. Progressive arc development from subduction initiation in the RSC to the Middle Jurassic arc that overprints the sutured Klamath terranes to the Rogue-Chetco arc all suggest continued subduction along this proto-Franciscan margin from the Late Triassic to the Middle Jurassic.

If the lower CMS subducted along this proto-Franciscan margin, it represents large scale coherent underplating in the early period of non-accretionary subduction. This period of subduction along the Franciscan margin (ca. 170-123 Ma) was previously assumed to only be preserved in high grade blocks and isolated slabs in the younger, lower grade melange of the Franciscan Central Belt. The onset of accretionary subduction was coincident with wide-scale underplating of the Franciscan Eastern Belt, increased sediment supply due to the rise of a laterally-continuous Cordilleran arc and Great Valley forearc and development of the accretionary wedge that is preserved in the Franciscan Complex (e.g., Dumitru et al., 2010; Orme & Surpless, 2019). Geochemical evidence from the lower CMS suggests incorporation of ultramafic and mafic lenses sourced from tectonic erosion of the overriding plate (Tewksbury-Christle et al., 2021), consistent with the early, non-accretionary Franciscan subduction margin. For example, the Scraggy Mountain epidote blueschist lens has an arc-affinity geochemical signature (Tewksbury-Christle et al., 2021) and a crystallization age comparable to the Western Hayfork arc, which occupied the hanging wall during subduction and is a possible source for the protolith of this blueschist lens.

Constraints on the early thermal structure of the Franciscan margin are difficult due to limited preservation and overprinting retrogression. The lower CMS preserves a coherently underplated record with limited retrogression that can be used to better constrain the early Franciscan conditions. Pressure-temperature (P-T) estimates from high grade blocks and slabs in the Central Belt suggest a wide range of geotherms (Cooper et al., 2011; Page et al., 2007; Massonne, 1995; Krogh Ravna & Terry, 2004; Krogh et al., 1994; Tsujimori et al., 2006; Wakabayashi, 1990; Ukar & Cloos, 2016). Geothermal gradients are better constrained in the coherently underplated Franciscan Eastern Belt (Fig. 7d) (Dumitru et al., 2010; Schmidt & Platt, 2020). We calculated the geotherm using the graphite crystallinity temperatures presented in this paper and previous pressure constraints (Tewksbury-Christle et al., 2021). The lower CMS fits broadly into the estimated geotherms and the cooling trend in the Franciscan Eastern Belt units. Further characterization of the lower CMS metamorphic history could provide further constraints and insights on early Franciscan subduction conditions.

6.3 Implications for mass and volatile recycling at erosive subduction margins

Our improved timing constraints have further implications for recycling of mass and volatiles to Earth's deep interior. Underplating in modern tectonically erosive margins is not currently accounted for in global mass and volatile budgets (e.g., Clift et al., 2009; Clift, 2017). Tewksbury-Christle et al. (2021) estimated that the lower CMS represents underplating of 10-60% of the incoming sediment despite subducting along a tectonically erosive margin. Uncertainty in underplating timing and duration, which affects the estimated sediment supply as well as the assumed plate velocities, drives the significant uncertainty in this estimate. With the new ages presented here, the onset of metamorphism near the top (ca. 133 Ma) and at the bottom (ca. 128 Ma) of the structural package brackets underplating duration for approximately 9 km of the lower CMS structural thickness. Using the cross sectional area and sediment supply rates calculated in Tewksbury-Christle et al. (2021) and Farallon plate velocities from Engebretson et al. (1985), in conjunction with our improved duration estimate, the lower CMS represents ca. 75% of the incoming sediment. This estimate is consistent with upper bounds of previous estimates of underplating percentages from Hikurangi (60%, calculated from Clift et al., 2009; Bassett et al., 2010), and the Andes (80%, Clift & Hartley, 2007). Significant preservation predicted for the lower CMS and other modern erosive margins suggests that underplating in erosive margins is an important factor to incorporate into mass and volatile budgets.

7 Conclusions

The western margin of North America records protracted underplating in the Klamath Mountains and the Franciscan Complex. Subduction during assembly of the Klamaths was characterized by fringing island arcs and terrane accretion and transitioned to Andean-style subduction resulting in the formation of the Franciscan Complex. This transition between the end of Klamath terrane accretion and the onset of coherent underplating in the Franciscan is poorly preserved due to a lack of accretion. The CMS is a subduction complex exhumed through a window in the overlying older Klamath terranes that records down-dip coherent underplating and up-dip tectonic erosion. Previously published age constraints on the upper CMS, in addition to regional structural relationships, suggest that the upper CMS can be correlated with other Klamath terranes (e.g., Klein, 1975; Saleeby & Harper, 1993). Previously published age constraints for the epidote-blueschist facies lower CMS, however, overlap with both the youngest Klamaths and oldest Franciscan.

We constrained lower CMS deposition/crystallization and emplacement using multiple geochronometers. Our geochronologic results constrain lower CMS deposition and subduction/underplating to 153-135 Ma and 119-133 Ma, respectively. These ages preclude direct correlation to both the youngest Klamath terranes (>150 Ma) and to the oldest, coherent Franciscan (underplated ca. 123 Ma). The lower CMS subducted after assembly of the other Klamath terranes, and subduction and emplacement began before and overlapped with underplating in the Francsican. P-T conditions in the lower CMS are consistent with other constraints from the early Franciscan history. Because the earliest Franciscan history is poorly preserved, efforts to reconstruct the thermal structure of the subduction margin rely on highly retrogressed isolated blocks and slabs. The lower CMS is a coherently underplated record of this transitional time frame with limited retrogression, and further characterization of CMS P-T conditions can provide further insights into evolution of the western North American margin.

Open Research Section

For the purposes of peer review, all data collected by the authors have been uploaded as excel files and indexed in the supplementary information. If this manuscript is accepted, the authors will submit the data to the ETH Research Collection, a publicly-accessible repository for research data and publications. These files will be publicly available and indexed with a DOI.

Acknowledgments
This work was supported by a National Science Foundation (NSF) CAREER Grant (EAR-1555346) and a European Research Council (ERC) Starting Grant (947659) awarded to W.M. Behr. We are deeply grateful to F. McDowell for the instrumental role he played in collection of the K-Ar data. We would also like to thank L. Stockli, M. Flansburg, and E. Poulaki for their exceptional help in mineral separation and LA-ICP-MS training, data reduction, and data interpretation for the detrital zircon analyses.

References

Allen, C. M., & Barnes, C. G. (2006). Ages and some cryptic sources of Mesozoic plutonic rocks in the Klamath Mountains, California and Oregon. *Geological Society of America Special Papers*, *410*, 223-245. doi: 10.1130/2006.2410(11)

Apen, F. E., Wakabayashi, J., Day, H. W., Roeske, S. M., Souders, A. K., & Dumitru, T. A. (2021). Regional-scale correlations of accreted units in the Franciscan Complex, California, USA: A record of long-lived, episodic subduction accretion. In *Plate Tectonics, Ophiolites, and Societal Significance of*

Geology: A Celebration of the Career of Eldridge Moores. Geological Society of America. doi: 10.1130/2021.2552(11)

Bachman, S. B. (1982). The coastal belt of the Franciscan: youngest phase of northern California subduction. *Geological Society, London, Special Publications*, *10*(1), 401–417. doi: 10.1144/gsl.sp.1982.010.01.27

Bailey, E. H., Irwin, W. P., & Jones, D. L. (1964). Franciscan and related rocks, and their significance in the geology of western California. *California Division of Mines and Geology Bulletin*, *183*, 1–177.

Barnes, C. G., Snoke, A. W., Harper, G. D., Frost, C. D., McFadden, R. R., Bushey, J. C., & Barnes, M. A. (2006). Arc plutonism following regional thrusting: Petrology and geochemistry of syn- and post-Nevadan plutons in the Siskiyou Mountains, Klamath Mountains province, California. *Geological Society of America Special Papers*, *410*, 357-376. doi: 10.1130/2006.2410(17)

Bassett, D., Sutherland, R., Henrys, S., Stern, T., Scherwath, M., Benson, A., ... Henderson, M. (2010). Three-dimensional velocity structure of the northern Hikurangi margin, Raukumara, New Zealand: Implications for the growth of continental crust by subduction erosion and tectonic underplating. *Geochemistry, Geophysics, Geosystems*, *11*(10), 1–24. doi: 10.1029/2010GC003137

Beyssac, O., Goffé, B., Chopin, C., & Rouzaud, J. N. (2002). Raman spectra of carbonaceous material in metasediments: a new geothermometer. *Journal of Metamorphic Geology*, *20*, 859–871. doi: 10.1046/j.1525-1314.2002.00408.x

Brown, E., & Blake, M. (1987). Correlation of early Cretaceous blueschists in Washington, Oregon and northern California. *Tectonics*, *6*(6), 795–806. doi: 10.1029/TC006i006p00795

Bushey, J. C., Snoke, A. W., Barnes, C. G., & Frost, C. D. (2006). Geology of the Bear Mountain intrusive complex, Klamath Mountains, California. *Geological Society of America Special Papers*, *410*, 287-315. doi: 10.1130/2006.2410(14)

Chapman, A. D., Yule, D., Schmidt, W., & LaMaskin, T. (2021). Middle Jurassic to Early Cretaceous tectonic evolution of the western Klamath Mountains and outboard Franciscan assemblages, northern California–southern Oregon, USA. In *From Terranes to Terrains: Geologic Field Guides on the Construction and Destruction of the Pacific Northwest.* Geological Society of America. doi: 10.1130/2021.0062(04)

Clift, P. (2017). A revised budget for Cenozoic sedimentary carbon subduction. *Reviews of Geophysics*, *55*(1), 97–125. doi: 10.1002/2016RG000531

Clift, P., & Hartley, A. J. (2007). Slow rates of subduction erosion and coastal underplating along the Andean margin of Chile and Peru. *Geology*, *35*(6), 503–506. doi: 10.1130/G23584A.1

Clift, P., Vannucchi, P., & Morgan, J. P. (2009). Crustal redistribution, crust–mantle recycling and Phanerozoic evolution of the continental crust. *Earth-Science Reviews*, *97*(1–4), 80–104. doi: 10.1016/j.earscirev.2009.10.003

Cloos, M. (1983). Comparative study of melange matrix and metashales from the Franciscan subduction complex with the basal Great Valley Sequence, California. *The Journal of Geology*, *91*(3), 291–306. doi: 10.1086/628772

Coleman, R., Helper, M., & Donato, M. (1983). Geologic Map of the Condrey Mountain Roadless Area, Siskiyou County, California. *U.S. Geological Survey, Miscellaneous Field Study Map MF-1540-A.*

Cooper, F. J., Platt, J. P., & Ancakiewicz, R. (2011). Constraints on early Franciscan subduction rates from 2-D thermal modeling. *Earth and Planetary Science Letters*, *312*(1-2), 69–79. doi: 10.1016/j.epsl.2011.09.051

Dickinson, W. R., & Gehrels, G. E. (2009). Use of U-Pb ages of detrital zircons to infer maximum depositional ages of strata: a test against a Colorado Plateau Mesozoic database. *Earth and Planetary Science Letters*, *288*(1-2), 115–125. doi: 10.1016/j.epsl.2009.09.013

Dumitru, T. A., Ernst, W., Wright, J. E., Wooden, J. L., Wells, R. E., Farmer,

L. P., . . . Graham, S. A. (2013). Eocene extension in Idaho generated massive sediment floods into the Franciscan trench and into the Tyee, Great Valley, and Green River basins. *Geology*, *41*(2), 187–190. doi: 10.1130/G33746.1

Dumitru, T. A., Wakabayashi, J., Wright, J. E., & Wooden, J. L. (2010). Early Cretaceous transition from nonaccretionary behavior to strongly accretionary behavior within the Franciscan subduction complex. *Tectonics*, *29*, 1–24. doi: 10.1029/2009TC002542

Engebretson, D. C., Cox, A., & Gordon, R. G. (1985). Relative motions between oceanic and continental plates in the Pacific Basin. *Geological Society of America Special Paper 206*, 1–58. doi: 10.1130/SPE206-p1

Ernst, W. G. (2015). Franciscan geologic history constrained by tectonic/olistostromal high-grade metamafic blocks in the iconic California Mesozoic-Cenozoic accretionary complex. *American Mineralogist*, *100*(1), 6–13. doi: 10.2138/am-2015-4850

Evitt, W. R., & Pierce, S. T. (1975). Early Tertiary ages from the coastal belt of the Franciscan complex, northern California. *Geology*, *3*, 433-436. doi: 10.1130/0091-7613(1975)3%3C433:ETAFTC%3E2.0.CO;2

Frost, C. D., Barnes, C. G., & Snoke, A. W. (2006). Nd and Sr isotopic data from argillaceous rocks of the Galice Formation and Rattlesnake Creek terrane, Klamath Mountains: Evidence for the input of Precambrian sources. *Geological Society of America Special Papers*, *410*, 103-120. doi: 10.1130/2006.2410(05)

Garcia, M. O. (1982). Petrology of the Rogue River island-arc complex, southwest Oregon. *American Journal of Science*, *282*(6), 783–807. doi: 10.2475/ajs.282.6.783

Gray, G. G. (1986). Native terranes of the central Klamath Mountains, California. *Tectonics*, *5*(7), 1043–1054. doi: 10.1029/TC005i007p01043

Gray, G. G. (2006). Structural and tectonic evolution of the western Jurassic belt along the Klamath River corridor, Klamath Mountains, California. *Geological Society of America Special Papers*, *410*, 141-151. doi: 10.1130/2006.2410(07)

Hacker, B. R., Donato, M. M., Barnes, C. G., McWilliams, M., & Ernst, W. (1995). Timescales of orogeny: Jurassic construction of the Klamath Mountains. *Tectonics*, *14*(3), 677–703. doi: 10.1029/94TC02454

Hamilton, W. (1969). Mesozoic California and the underflow of Pacific mantle. *Geological Society of America Bulletin*, *80*(12), 2409–2430. doi: 10.1130/0016-7606(1969)80%5B2409:MCATUO%5D2.0.CO;2

Harper, G. D. (2006). Structure of syn-Nevadan dikes and their relationship to deformation of the Galice Formation, western Klamath terrane, northwestern California. *Geological Society of America Special Papers*, *410*, 121-140. doi: 10.1130/2006.2410(06)

Harper, G. D., Saleeby, J. B., & Heizler, M. (1994). Formation and emplacement of the Josephine ophiolite and the Nevadan orogeny in the Klamath Mountains, California-Oregon: U/Pb zircon and ^{40}Ar/^{39}Ar geochronology. *Journal of Geophysical Research: Solid Earth*, *99*(B3), 4293–4321. doi: 10.1029/93JB02061

Helper, M. (1985). *Structural, metamorphic and geochronologic constrains on the origin of the Condrey Mountain Schist, north central Klamath Mountains, northern California* (Doctoral dissertation, University of Texas at Austin). doi: 10.1029/93JB02061

Helper, M. (1986). Deformation and high P/T metamorphism in the central part of the Condrey Mountain window, north-central Klamath Mountains, California and Oregon. *GSA Memoir 164*, 125–142. doi: 10.1130/MEM164-p125

Hill, L. B. (1985). Metamorphic, deformational, and temporal constraints on terrane assembly, northern Klamath Mountains, California. *Tectonostratigrahic Terranes of the Circum-Pacific Region, Earth Science Series*.

Hopson, C. A., Mattinson, J. M., Pessagno, E. A., & Luyendyk, B. P. (2008). California Coast Range ophiolite: Composite Middle and Late Jurassic oceanic lithosphere. *Geological Society of America Special Papers*, *438*, 1-102. doi: 10.1130/2008.2438(01)

Hoskin, P. W. (2005). Trace-element composition of hydrothermal zircon and the alteration of Hadean zircon from the Jack Hills, Australia. *Geochimica et Cosmochimica Acta*, *69*(3), 637–648. doi: 10.1016/j.gca.2004.07.006

Hoskin, P. W., & Schaltegger, U. (2003). The composition of zircon and igneous and metamorphic petrogenesis. *Reviews in mineralogy and geochemistry*, *53*(1), 27–62. doi: 10.2113/0530027

Irwin, W. P. (1972). Terranes of the western Paleozoic and Triassic belt in the southern Klamath Mountains, California. In *Usgs professional paper 800-c* (p. C103-C111).

Jackson, S. E., Pearson, N. J., Griffin, W. L., & Belousova, E. A. (2004). The application of laser ablation-inductively coupled plasma-mass spectrometry to in situ U-Pb zircon geochronology. *Chemical Geology*, *211*(1-2), 47–69. doi: 10.1016/j.chemgeo.2004.06.017

Jäger, E. (1979). Introduction to geochronology. In *Lectures in isotope geology* (pp. 1–12). Springer. doi: 10.1007/978-3-642-67161-6_1

Jayko, A., & Blake Jr, M. (1986). Significance of Klamath rocks between the Franciscan Complex and Coast Range ophiolite, northern California. *Tectonics*, *5*(7), 1055–1071. doi: 10.1029/TC005i007p01055

Kirkland, C., Smithies, R., Taylor, R., Evans, N., & McDonald, B. (2015). Zircon Th/U ratios in magmatic environs. *Lithos*, *212*, 397–414. doi: 10.1016/j.lithos.2014.11.021

Klein, C. W. (1975). *Structure and petrology of a southeastern potion of the Happy Camp Quadrangle, Siskyou County, northwest California* (Unpublished doctoral dissertation). Harvard University.

Krogh, E., Oh, C., & Liou, J. (1994). Polyphase and anticlockwise P-T evolution for Franciscan eclogites and blueschists from Jenner, California, USA. *Journal of Metamorphic Geology*, *12*(2), 121–134. doi: 10.1111/j.1525-1314.1994.tb00008.x

Krogh Ravna, E., & Terry, M. P. (2004). Geothermobarometry of UHP and HP eclogites and schists–an evaluation of equilibria among garnet–clinopyroxene–kyanite–phengite–coesite/quartz. *Journal of Metamorphic Geology*, *22*(6), 579–592. doi: 10.1111/j.1525-1314.2004.00534.x

LaMaskin, T. A., Rivas, J. A., Barbeau, J., David L., Schwartz, J. J., Russell, J. A., & Chapman, A. D. (2021). A crucial geologic test of Late Jurassic exotic collision versus endemic re-accretion in the Klamath Mountains Province, western United States, with implications for the assembly of western North America. *GSA Bulletin*, *134*(3-4), 965-988. doi: 10.1130/B35981.1

Lanphere, M. A., Irwin, W. P., & Hotz, P. E. (1968). Isotopic age of the Nevadan orogeny and older plutonic and metamorphic events in the Klamath Mountains, California. *Geological Society of America Bulletin*, *79*(8), 1027–1052. doi: 10.1130/0016-7606(1968)79%5B1027:IAOTNO%5D2.0.CO;2

Macdonald, J. H. J., Harper, G. D., & Zhu, B. (2006). Petrology, geochemistry, and provenance of the Galice Formation, Klamath Mountains, Oregon and California. *Geological Society of America Special Papers 410*, 77–101. doi: 10.1130/2006.2410(04)

Marsh, J. H., & Stockli, D. F. (2015). Zircon U-Pb and trace element zoning characteristics in an anatectic granulite domain: Insights from LASS-ICP-MS depth profiling. *Lithos*, *239*, 170–185. doi: 10.1016/j.lithos.2015.10.017

Massonne, H.-J. (1995). Experimental and petrogenetic study of UHPM. In R. G. Coleman & X. Wang (Eds.), *Ultrahigh Pressure Metamorphism* (p. 33–95). Cambridge University Press. doi: 10.1017/CBO9780511573088.003

Massonne, H.-J., & Schreyer, W. (1987). Phengite geobarometry based on the limiting assemblage with K-feldspar, phlogopite, and quartz. *Contributions to Mineralogy and Petrology*, *96*, 212–224. doi: 10.1007/BF00375235

McFadden, R. R., Snoke, A. W., & Barnes, C. G. (2006). Structural and petrologic evolution of the Bear Peak intrusive complex, Klamath Mountains, California. *Geological Society of America Special Papers*, *410*, 333-355. doi: 10.1130/2006.2410(16)

Morissani, A. M. (2006). *Detrital zircon geochronology and petrography of Franciscan graywacke blocks at San Simeon, California: implications for melange genesis* (Unpublished doctoral dissertation). University of Texas at Austin.

Mortimer, N., & Coleman, R. (1985). A Neogene structural dome in the Klamath Mountains, California and Oregon. *Geology*, *13*, 253–256. doi: 10.1130/0091-7613(1985)13%3C253:ANSDIT%3E2.0.CO;2

Nilsen, T. H. (1984). Stratigraphy, sedimentology, and tectonic framework of the Upper Cretaceous Hornbrook Formation, Oregon and California. *Pacific Section SEPM*, *42*, 51–88.

Orme, D. A., & Surpless, K. D. (2019, 06). The birth of a forearc: The basal Great Valley Group, California, USA. *Geology*, *47*(8), 757-761. doi: 10.1130/G46283.1

Page, F. Z., Armstrong, L. S., Essene, E. J., & Mukasa, S. B. (2007). Prograde and retrograde history of the Junction School eclogite, California, and an evaluation of garnet–phengite–clinopyroxene thermobarometry. *Contributions to Mineralogy and Petrology*, *153*(5), 533–555. doi: 10.1007/s00410-006-0161-9

Paton, C., Woodhead, J. D., Hellstrom, J. C., Hergt, J. M., Greig, A., & Maas, R. (2010). Improved laser ablation U-Pb zircon geochronology through robust downhole fractionation correction. *Geochemistry, Geophysics, Geosystems*, *11*(3). doi: 10.1029/2009GC002618

Pessagno, E. A. (2006). Faunal evidence for the tectonic transport of Jurassic terranes in Oregon, California, and Mexico. *Geological Society of America Special Papers*, *410*, 31-52. doi: 10.1130/2006.2410(02)

Petrus, J. A., & Kamber, B. S. (2012). VizualAge: A novel approach to laser ablation ICP-MS U-Pb geochronology data reduction. *Geostandards and Geoanalytical Research*, *36*(3), 247–270. doi: 10.1111/j.1751-908X.2012.00158.x

Piotraschke, R., Cashman, S. M., Furlong, K. P., Kamp, P. J., Danišík, M., & Xu, G. (2015). Unroofing the Klamaths—Blame it on Siletzia? *Lithosphere*, *7*(4), 427–440. doi: 10.1130/L418.1

Platt, J. P. (2015). Origin of Franciscan blueschist-bearing melange at San Simeon, central California coast. *International Geology Review*, *57*(5-8), 843–853. doi: 10.1080/00206814.2014.902756

Poulaki, E. M., Stockli, D. F., Flansburg, M. E., Gevedon, M. L., Stockli, L. D., Barnes, J. D., ... Valley, J. W. (2021). Zircon U-Pb and geochemical signatures in high-pressure, low-temperature metamorphic rocks as recorders of subduction zone processes, Sikinos and Ios islands, Greece. *Chemical Geology*, *582*, 120447. doi: 10.1016/j.chemgeo.2021.120447

Rubatto, D. (2017). Zircon: the metamorphic mineral. *Reviews in Mineralogy and Geochemistry*, *83*(1), 261–295. doi: 10.2138/rmg.2017.83.9

Ruffet, G., Gruau, G., Ballèvre, M., Féraud, G., & Philippot, P. (1997). Rb-Sr and ^{40}Ar-^{39}Ar laser probe dating of high-pressure phengites from the Sesia zone (Western Alps): underscoring of excess argon and new age constraints on the high-pressure metamorphism. *Chemical Geology*, *141*(1-2), 1–18. doi: 10.1016/S0009-2541(97)00052-1

Saleeby, J. B. (1990). Geochronological and tectonostratigraphic framework of Sierran-Klamath ophiolitic assemblages. *Geological Society of America Special Papers*, *255*, 93-114. doi: 10.1130/SPE255-p93

Saleeby, J. B., & Harper, G. D. (1993). Tectonic relations between the Galice Formation and the Condrey Mountain Schist, Klamath Mountains, northern

California. *Mesozoic Paleogeography of the Western United States-II*.
Scaillet, S. (1998). K-Ar ($^{40}Ar/^{39}Ar$) geochronology of ultrahigh pressure rocks. In *When continents collide: Geodynamics and geochemistry of ultrahigh-pressure rocks* (pp. 161–201). Springer. doi: 10.1007/978-94-015-9050-1_7
Schmidt, W. L., & Platt, J. P. (2018). Subduction, accretion, and exhumation of coherent Franciscan blueschist-facies rocks, northern Coast Ranges, California. *Lithosphere*, *10*(2), 301–326. doi: 10.1130/L697.1
Schmidt, W. L., & Platt, J. P. (2020). Metamorphic temperatures and pressures across the eastern franciscan: Implications for underplating and exhumation. *Lithosphere*, *2020*(1). doi: 10.2113/2020/8853351
Sharman, G. R., Graham, S. A., Grove, M., Kimbrough, D. L., & Wright, J. E. (2015). Detrital zircon provenance of the Late Cretaceous-Eocene California forearc: Influence of Laramide low-angle subduction on sediment dispersal and paleogeography. *Bulletin*, *127*(1-2), 38–60. doi: 10.1130/B31065.1
Shervais, J. W., & Choi, S. H. (2012). Subduction initiation along transform faults: The proto-Franciscan subduction zone. *Lithosphere*, *4*(6), 484–496. doi: 10.1130/L153.1
Sláma, J., Košler, J., Condon, D. J., Crowley, J. L., Gerdes, A., Hanchar, J. M., ... Whitehouse, M. J. (2008). Plešovice zircon—a new natural reference material for U-Pb and Hf isotopic microanalysis. *Chemical Geology*, *249*(1-2), 1–35. doi: 10.1016/j.chemgeo.2007.11.005
Snoke, A. W., & Barnes, C. G. (2006). The development of tectonic concepts for the Klamath Mountains province, California and Oregon. *Geological Society of America Special Papers 410*, 1–29. doi: 10.1130/2006.2410(01)
Suppe, J., & Armstrong, R. L. (1972). Potassium-argon dating of Franciscan metamorphic rocks. *American Journal of Science*, *272*(3), 217–233. doi: 10.2475/ajs.272.3.217
Surpless, K. D., Alford, R. W., Barnes, C., Yoshinobu, A., & Weis, N. E. (2023). Late Jurassic paleogeography of the US Cordillera from detrital zircon age and hafnium analysis of the Galice Formation, Klamath Mountains, Oregon and California, USA. *GSA Bulletin*. doi: 10.1130/B36810.1
Tewksbury-Christle, C. M., Behr, W. M., & Helper, M. A. (2021). Tracking deep sediment underplating in a fossil subduction margin: Implications for interface rheology and mass and volatile recycling. *Geochemistry, Geophysics, Geosystems*, *22*(3). doi: 10.1029/2020GC009463
Tomaschek, F., Kennedy, A. K., Villa, I. M., Lagos, M., & Ballhaus, C. (2003). Zircons from Syros, Cyclades, Greece—recrystallization and mobilization of zircon during high-pressure metamorphism. *Journal of Petrology*, *44*(11), 1977–2002. doi: 10.1093/petrology/egg067
Tsujimori, T., Matsumoto, K., Wakabayashi, J., & Liou, J. (2006). Franciscan eclogite revisited: Reevaluation of the P–T evolution of tectonic blocks from Tiburon Peninsula, California, USA. *Mineralogy and Petrology*, *88*(1-2), 243. doi: 10.1007/s00710-006-0157-1
Ukar, E. (2012). Tectonic significance of low-temperature blueschist blocks in the Franciscan mélange at San Simeon, California. *Tectonophysics*, *568*, 154–169. doi: 10.1016/j.tecto.2011.12.039
Ukar, E., & Cloos, M. (2016). Graphite-schist blocks in the Franciscan Mélange, San Simeon, California: Evidence of high-P metamorphism. *Journal of Metamorphic Geology*, *34*(3), 191–208. doi: 10.1111/jmg.12174
Vermeesch, P. (2004). How many grains are needed for a provenance study? *Earth and Planetary Science Letters*, *224*(3-4), 441–451. doi: 10.1016/j.epsl.2004.05.037
Wakabayashi, J. (1990). Counterclockwise P-T-t paths from amphibolites, Franciscan Complex, California: Relics from the early stages of subduction zone metamorphism. *The Journal of Geology*, *98*(5), 657–680. doi: 10.1086/629432

Wakabayashi, J. (2015). Anatomy of a subduction complex: Architecture of the Franciscan Complex, California, at multiple length and time scales. *International Geology Review*, *57*(5-8), 669–746. doi: 10.1080/00206814.2014.998728

Wakabayashi, J., & Dumitru, T. A. (2007). ^{40}Ar/^{39}Ar ages from coherent, high-pressure metamorphic rocks of the Franciscan Complex, California: Revisiting the timing of metamorphism of the world's type subduction complex. *International Geology Review*, *49*(10), 873–906. doi: 10.2747/0020-6814.49.10.873

Watson, E., Wark, D., & Thomas, J. (2006). Crystallization thermometers for zircon and rutile. *Contributions to Mineralogy and Petrology*, *151*(4), 413. doi: 10.1007/s00410-006-0068-5

Wiedenbeck, M., Alle, P., Corfu, F., Griffin, W., Meier, M., Oberli, F. v., ... Spiegel, W. (1995). Three natural zircon standards for U-Th-Pb, Lu-Hf, trace element and REE analyses. *Geostandards Newsletter*, *19*(1), 1–23. doi: 10.1111/j.1751-908X.1995.tb00147.x

Wright, J. E. (1982). Permo-Triassic accretionary subduction complex, southwestern Klamath Mountains, northern California. *Journal of Geophysical Research: Solid Earth*, *87*(B5), 3805–3818. doi: 10.1029/JB087iB05p03805

Wright, J. E., & Wyld, S. J. (1994). The Rattlesnake Creek terrane, Klamath Mountains, California: An early Mesozoic volcanic arc and its basement of tectonically disrupted oceanic crust. *Geological Society of America Bulletin*, *106*(8), 1033–1056. doi: 10.1130/0016-7606(1994)106%3C1033:TRCTKM%3E2.3.CO;2

Yakymchuk, C., Kirkland, C. L., & Clark, C. (2018). Th/U ratios in metamorphic zircon. *Journal of Metamorphic Geology*, *36*(6), 715–737. doi: 10.1111/jmg.12307

Yule, J. D., Saleeby, J. B., & Barnes, C. G. (2006). A rift-edge facies of the Late Jurassic Rogue-Chetco arc and Josephine ophiolite, Klamath Mountains, Oregon. *Geological Society of America Special Papers*, *410*, 53-76. doi: 10.1130/2006.2410(03)